Conjugated Small Molecules: A Promising Hole Transport Materials in Perovskite Photovoltaics

I. V. Martynov, A.N. Zhivchikova, M. D. Tereshchenko, I. E. Kuznetsov, M.M. Tepliakova, A. V. Akkuratov.*

A.N. Zhivchikova, M.M. Tepliakova,
Skolkovo Institute of Science and Technology, 3 Nobel str., Moscow,
143026, Moscow, Russian Federation

M. D. Tereshchenko, I. E. Kuznetsov, A. V. Akkuratov.
Federal Research Center of Problems of Chemical Physics and Medicinal Chemistry, Russian Academy of Sciences. FRC PCPMC RAS, Academician Semenov avenue 1, Chernogolovka, 142432, Moscow region, Russian Federation

M. D. Tereshchenko.
Perm National Research Polytechnic University, PNIPU, Komsomolsky pr., 29, Perm, 614990 Perm region, Russian Federation

I. V. Martynov,*

Center for Photonics and 2D Materials, Moscow Institute of Physics and Technology, 14170 Dolgoprudny, Russia; E-mail: martinov@mitht.org

Keywords: triphenylamine, hole-transport materials, organic semiconductor materials, hole mobility, perovskite solar cells

There is a resurgence in the use of triphenylamine-based donor materials (TPA) in the field of perovskite photovoltaics. This work presents the synthesis of two novel conjugated small molecules (CSM's), TPA-t and TPA-t EH, which are functionalized with triisopropylsilyl groups and 2-ethylhexyl side chains. These molecules show promise as hole transport materials, which possess high hole mobilities of 1.5×10^{-4} and 2.9×10^{-3} cm^2 V^{-1} s^{-1} due to self-organization. TPA-t and TPA-t EH possess HOMO energy levels at -5.38 and -5.31 eV, which is well-aligned with valence band of standard perovskite $MAPbI_3$.This resulted in outstanding

open-circuit voltages of 1100 and 1080 mV. TPA-based molecules were investigated as HTLs in n-i-p PSCs without additional doping and enabled high efficiency (17.4 %) same as for devices with state-of-the-art polytriarylamine (PTAA) HTL. The obtained results suggest that developed materials could potentially compete with PTAA when further material structure modification.

Introduction

Perovskite solar cells (PSC's) is a rapidly developing photovoltaic technology that can compete with silicon solar cells and gain a strong position in the market. [1] Over the course of the previous decade, the energy conversion efficiency (PCE) of single-junction PSCs has undergone a significant increase rising from 14% to 26.1%. [2–4] This notable growth can be attributed to the interest of researchers in the exceptional characteristics of metal-halide perovskite, such as its substantial absorption coefficients, high mobilities, long diffusion lengths, and the ability to tune crystalline thin films. Solar cells that are based on perovskite materials possess numerous advantages, including a straightforward manufacturing process, the ability to customize optical and electrical properties, a low cost of active materials, and the opportunity to optimize the device structure. Additionally, there is potential for the development of new absorbing materials. [5–7] However, a major barrier to their commercialization is the problem of weak stability. The interaction between the active layer and moisture is the main source of the PSC's instability, though other layers and interfaces also play a role in the device's overall degradation. Researchers have tried a number of methods to increase the stability of PSC's, such as creating new hole transfer layers (HTL), modifying interfaces, developing new material compositions, and investigating novel device arrangements.[8,9] Design of new hole transfer layers is a promising strategy to improve PSC stability. Spiro-OMeTAD and PTAA, which are currently the most widely used HTL's in PSC's provide still the highest efficiency in n-i-p architectures. [10,11] Furthermore, recent research has demonstrated that the primary factors limiting stability and efficiency in highly efficient n-i-p PSCs are the charge transfer characteristics at the perovskite/HTL interface. [12–15] In order for the developed new HTL materials to have prospects for use in PSC's, they have to meet the following criteria: (1) matching the energy level of the perovskite appropriately to extract holes and block electrons; (2) high conductivity and mobility of holes; (3) high solubility, which helps the formation of a film morphology free of pinholes and smooth; (4) good stability; and (5) low cost. [16,17] Recent research has demonstrated that highly ordered molecular packing is typically responsible for the high charge mobility of conjugated small molecules (CSM's). CSM's are regarded as

promising semiconductor materials because they comprise flexible alkyl side chains and rigid conjugated blocks. These substances have adjustable optical and electrical characteristics along with good solubility. [18,19] Due to the presence of broad peripheral wings, starburst-shaped compounds are generally thought to recrystallize less than linear analogs. One frequently used component in small-molecular p-type organic semiconductors is the triphenylamine (TPA) moiety. TPA-based small molecules have reasonable hole-transporting capabilities because of their strong donor ability. However, the TPA unit's propeller-like molecular structure typically produced soluble but amorphous materials. [20–22]

Triisopropylsilyl and 2-ethylhexyl side chains were used to functionalize the terminal thiophene rings of novel materials to improve their solubility and crystallinity in the solid state, because the π-π stacking and planarity of molecules are improved by a C−Si bond length than a C−C bond.

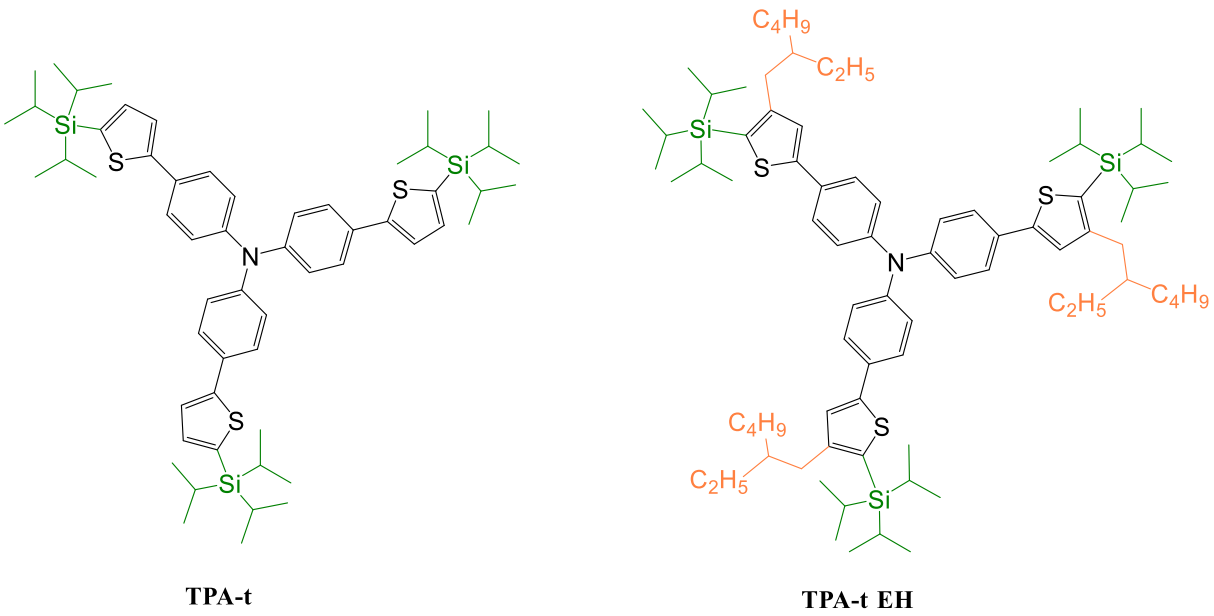

Figure 1. Molecular structures of developed molecules **TPA-t**, **TPA-t EH**.

Experimental Section

UV–Vis absorption measurements

Absorption spectra for dilute solutions of small molecules (1×10^{-4} M) and thin films deposited by spin-coating from 1×10^{-2} M solutions on quartz substrates were measured in UV-visible region (300-800 nm) on fiber optical spectrometer OPTOSKY ATP 2400.

Thermal properties

Thermal gravimetry analysis (TGA) using Q50 TA instruments under nitrogen with a heating rate of 10 °C min^{-1}. Differential scanning calorimetry (DSC) was performed using Netzsch DSC 214 Polyma instrument at the same conditions.

Cyclic voltammetry measurements

Electrochemical measurements were performed for thin films of the small molecules deposited on a glassy carbon disc electrode by drop casting from chloroform. The measurements were performed in a three-electrode electrochemical cell using a 0.1 M solution of Bu_4NBF_4 in acetonitrile as a supporting electrolyte, platinum wire as a counter electrode and Ag/Ag^+ (in 0.01 M acetonitrile) as a reference electrode. Ferrocene was used as an internal reference. The voltammograms were recorded using an ELINS P-20X instrument at room temperature in the range from −0.4 to 1.0 V with a potential sweep rate of 50 mV s^{-1}. [23]

Hole mobility measurements

SCLC devices were fabricated on glass substrates with photo-lithographically defined bottom ITO electrode. PEDOT:PSS (PH 1000, Heraues Clevios) was deposited by spin-coating. The substrates were subsequently dried at 160 °C for 10 min. Compounds TPA-t and TPA-t EH were deposited by spin-coating from chloroform solutions giving film thicknesses in the range of 150–230 nm. After that, MoO_x and Ag were successively deposited by thermal evaporation in a vacuum chamber (6×10^{-6} mbar) to form the top electrode. The same procedure was performed for devices, where the films were additionally annealed at 150 °C. The film thickness was recorded by making a thin scratch on the top of films. Subsequently, the AFM was scanned across the cut and the film thickness could thus be extracted from the resulting image.

Characterization of bilayer stacks

The atomic force microscopy (AFM) and Kelvin probe force microscopy (KPFM) imaging were carried to characterize morphology of perovskite/HTL thin films using the Scanning Probe Microscope Cypher EX (Asylum Research).

The time-resolved PL measurements was performed with TCSPC time correlated single photon counter technique on Horiba QuantaMaster spectrofluorimeter. The normalized PL decay curves are presented in a logarithmic scale.

Device fabrication

Prior to ETL deposition, glass/ITO substrates were cleaned with sonication in water, acetone, and isopropanol, dried in N_2 flow, then were put to an air plasma chamber at 50W for 15 min. SnO_2 electron-transport layer was formed from 10% aqueous tin oxide (IV) colloidal dispersion using dynamic spin-coating at 4000 rpm for 30 s, and then annealed at 175°C for 15 min. The hot substrates were transferred to inert (N_2) atmosphere of glovebox followed by annealing at

150°C for 10 min. PCBA was deposited from 0.4 mg mL^{-1} chlorobenzene solution statically at 3000 rpm, then heated at 100°C for 10 min. After that, the perovskite precursor (1.4 M MAI, 1.4 M PbI_2 in 4:1 DMF:NMP mixture) was deposited in a single-step technique at 4000 rpm dynamically. The $MAPbI_3$ crystallization was triggered by the toluene (150 μL at 18 s) antisolvent dripping followed by the substrate rotating for 40 s. The samples were left to rest for 15 min. Black substrates were slowly heated up to 80°C and annealed at this temperature for 5 min. The reference HTM PTAA was deposited from 6 mg mL^{-1} chlorobenzene solution at 4000 rpm for 15 s on cool substrates. The small-molecule HTLs were deposited from pre-heated to 90°C 7 mg mL^{-1} chlorobenzene solutions. The deposition conditions of all materials were optimized in preliminary experiments. Thicknesses of PTAA and HTLs were measured using AFM and are in the range of 15 ± 5 nm. The MoO_x (11 nm) and Ag (100 nm) layers were thermally evaporated under reduced pressure (10^{-5} mbar).

Device characterization

The efficiency of the devices was determined with the current-voltage (*J*–V) characterization under simulated 100 mW cm^2 AM 1.5G solar irradiation provided by the Newport Verasol AAA class solar simulator. The silicon diode with documented spectral response served as a standard for calibration. Current-voltage dependencies were recorded under N_2 atmosphere using Kethley 2400 source-measurement unit. The active electrode area of the solar cells was defined with the 0.08 cm^2 shadow mask.

The EQE spectra were measured using QEXL External Quantum Efficiency Measurement System (USA) in an inert atmosphere.

Results and discussion

The structures of TPA-based compounds **TPA-t** and **TPA-t EH** are depicted in **Figure 1**, and the detailed synthetic route is shown in **Scheme 1**. Bromination of triphenylamine with N-bromosuccinimide (NBS) afforded tris(4-bromophenyl)amine (**1**). Stille cross-coupling reaction between compound **1** and tributyl(thien-2-yl)stannane resulted in compound **2**, which was lithiated with n-BuLi followed by the addition of tri(2-propyl)cholorosilane, thus giving desired product **TPA-t**. The synthesis of **TPA-t EH** started with preparation of compound **3** by Kumada reaction of 3-bromothiophene with 3-(2-ethylhexyl)magnesium bromide. The bromination of **3** with NBS led to compound **4**, which was converted into (3-(2-ethylhexyl)thiophen-2-yl)triisopropylsilane (**5**). Compound **5** was lithiated and then treated with trimethylchlorostannane to obtain (5-(trimethylstannyl)thiophen-2-yl)triisopropylsilane (**6**). **TPA-t_EH** was synthesized by Stille reaction using compounds **1** and **6**. Both small

molecules were purified by column chromatography and multiple recrystallization from 2-propanol. According to HPLC data, the purity of **TPA-t** and **TPA-t EH** was about 99%.

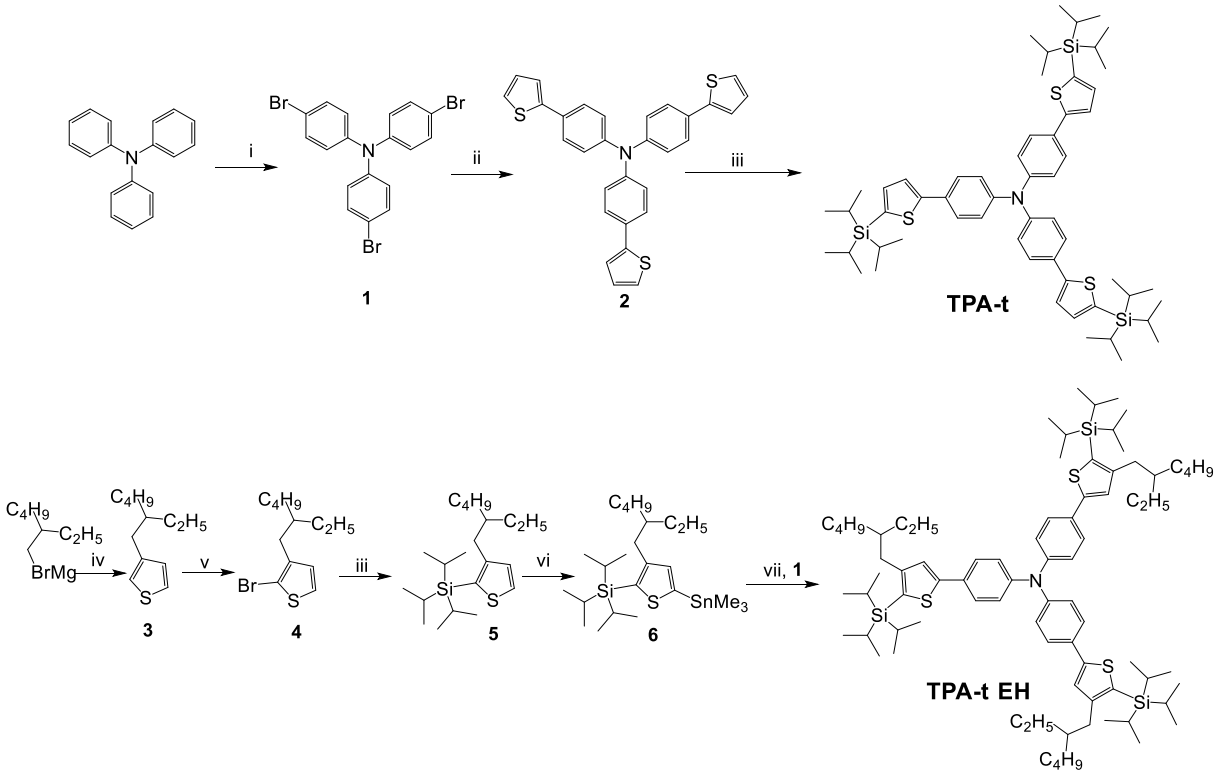

Scheme 1. Synthesis of small molecules **TPA-t** and **TPA-t EH**. Conditions: i – NBS, DMF; ii – tributyl(thien-2-yl)stannane, $Pd(PPh)_3$, DMF, 150°C; iii – n-BuLi, THF, $(i\text{-}Pr)_3SiCl$; iv – 3-bromothophene, $Ni(dppf)Cl_2$, THF; v – NBS, AcOH; vi – n-BuLi, THF, Me_3SnCl; vii – $Pd(PPh)_3$, DMF, 150°C.

The normalized UV-Vis absorption spectra for **TPA-t** and **TPA-t EH** in dichloromethane solution and solid films are shown in **Figure 2a** and the corresponding data is summarized in Table 1. In diluted solution **TPA-t** and **TPA-t EH** display a narrow absorption band with maxima peaks at 375 and 378 nm, respectively, which is attributed to the delocalized excitonic π- π* transition. The absorption spectra for films are similar, although the bands are slightly red-shifted to 376 and 380 nm. [24,25] These results may suggest that small molecules at the room temperature already exhibit strong aggregation in solutions, irrespective of the presence or absence of solubilizing alkyl chains (**TPA-t EH** or **TPA-t**, respectively).[26–28] The photoluminescence spectra of thin films show similar narrow emission bands with peak maxima around 460 nm for both molecules (see **Figure S1** in the Supporting Information). We calculated the optical band gap energies (E_g^{opt}) of the small molecules using the onset wavelengths of absorption bands in film spectra. Table 1 shows that the E_g^{opt} values for **TPA - t**

and **TPA-t EH** is 2.9 eV. The identical band gap values suggest that the TPA core predominantly influences these molecules, likely due to high molecular aggregation.

Table 1. Optical, electrochemical, and thermal properties of compounds **TPA-t** and **TPA – t EH**.

HTM	λ_{max}^{sol}, [nm][a)]	λ_{max}^{film} [nm][a)]	E_g^{opt}, [eV][b)]	E_{onset}^{ox}, [V vs. Fc^+/Fc]	HOMO, [eV][c)]	LUMO, [eV][d)]	T_d, [°C]	T_m/T_c, [°C]
TPA-t	375	376	2.9	0.58	-5.38	-2.48	358	228/188
TPA-t EH	378	380	2.9	0.51	-5.31	-2.41	343	-/106

a) Absorption maxima of the UV–vis spectra in solution and thin film.
b) Optical band gap determined by λ_{onset} ($E_g^{opt} = 1240/\lambda_{onset}$).
c) $E_{HOMO} = -(E_{onset}$ ox vs. $Fc/Fc^+ + 4.8)$, eV
d) LUMO is calculated from HOMO energy levels and optical band gaps

The Cyclic Voltammograms (CV) for thin films of **TPA-t** and **TPA-t EH** are depicted in **Figure 2b**. The highest occupied molecular orbital (HOMO) energy levels were calculated as HOMO = − (E_{onset}^{ox} + 4.8) eV, where the oxidation potentials (E_{onset}^{ox}) were determined by the onsets of the first oxidation waves. The electrodes were calibrated against the ferrocene/ferrocenium couple as a standard. [29] As previously demonstrated, the alkylsilyl functionalization of the organic semiconductor to provide deep the HOMO energy, what is observed to **TPA-t** (- 5.38eV)[30]. On the other hand, introducing an ethylhexyl side chain into **TPA-t EH** increases HOMO by 0.07 eV compared to **TPA-t**. The optoelectronic properties of **TPA-t** and **TPA-t EH** make them promising p-type semiconductor materials for organic and hybrid photovoltaics. These compounds are also suitable for using as hole transport materials in perovskite solar cells due to their well-aligned energy levels with $MAPbI_3$.

The thermal properties of the designed molecules were studied using thermal gravimetry analysis (TGA) and differential scanning calorimetry (DSC). The decomposition temperatures are 358 °C and 343 °C for **TPA-t** and **TPA-t EH**, respectively (see Figure 2c). This suggests that the materials are highly resistant to heat stress. However, it should be noted that TPA-t EH begins to partially destruct at lower temperatures than **TPA-t**. The melting point was registered at 228°C only for **TPA-t**, according to the DSC analysis. After cooling from the isotropic liquid phase, no signal was detected, indicating an amorphous solid phase for both materials. An exothermic peak appeared on the heating curve at 106°C and 183°C for **TPA-t** and **TPA-t EH** respectively, suggesting a cold crystallization process. A similar tendency towards

crystallization was observed in other small molecules, including those where terminal thiophene rings were functionalized with tributylsilyl groups.[31]

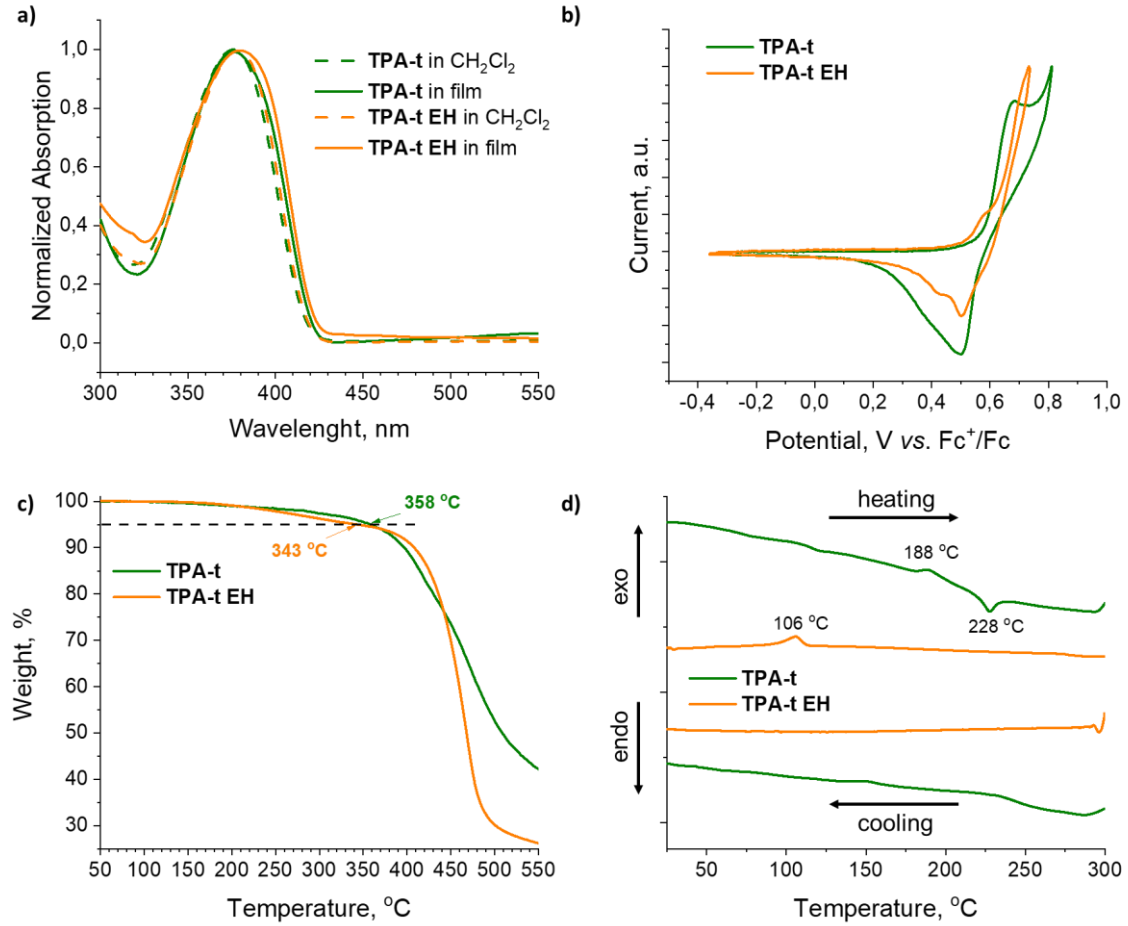

Figure 2. Absorption spectra in solution and thin films of **TPA-t** and **TPA-t EH** (a); CV curves for thin films in 0.1 M Bu_4NPF_6 in acetonitrile at scan rate of 50 mV s^{-1} (b); DSC thermograms (c) and TGA plots (d) measured in inert atmosphere.

We studied the charge transport properties of synthesized small molecules to assess their potential as hole transport materials. The hole mobilities were measured in hole-only devices (ITO/PEDOT : PSS/**HTM**/MoO_x/Ag) using the space-charge limited current method (SCLC).[32,33] The *J*-V curves for devices with **TPA-t** and **TPA-t EH** films are presented in **Figure 3a**. The estimated hole mobilities for **TPA-t** and **TPA-t EH** are 1.5×10^{-4} and 2.9×10^{-3} $cm^2\ V^{-1}\ s^{-1}$, respectively. The higher μ_h values obtained for **TPA-t EH** can be attributed to a lower number of defects on the bulk film. However, the hole mobility for **TPA t** is of the one order higher as the mobility for the PTAA known as the standard used HTM. [10,34]These results highlight the promise of synthesized materials due to their high hole mobility.

The hole transfer ability and interfacial charge transfer dynamics were further studied using time-resolved photoluminescence (TRPL) in two-layer structures perovskite/HTL. TRPL decay time (τ) in perovskite/HTM bilayer films indicates hole transfer from the conduction band of the perovskite into the HOMO level of the HTM.

The interfacial charge transfer dynamics were analyzed using TRPL experiments. The obtained curves were fitted with a bi-exponential decay model (Figure 3b, Table S1). In the two temporal regimes the faster decay τ_1 is attributed to charge transfer from the perovskite to the HTL or parasitic Shockley-Read-Hall recombination. The slower component τ_2 is ascribed to bimolecular recombination.[35,36] Compared with a neat perovskite layer with **TPA-t**, we found a significantly shorter τ_1 lifetime, 7 ns compared to 20 ns for pure perovskite. (Table S1). We interpret this as a quick charge transfer process from perovskite to HTL, which reduces radiation recombination. Adding a **TPA-t EH** layer to the perovskite does not alter the τ_1 lifetime, which may indicate a more limited charge transfer at probable parasitic recombination on the interface. However, when comparing the slower sections of τ_2, an opposite trend is observed. The τ_2 lifetime is longer for **TPA-t EH** compared to **TPA-t**, correlating with fewer traps in this HTM volume and the high hole mobility in this material.

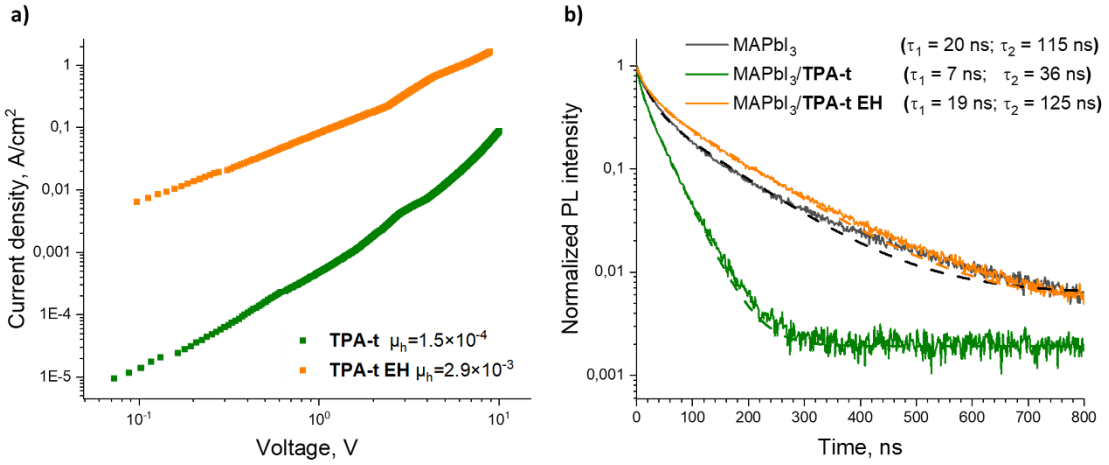

Figure 3. Space-charge limited current method (SCLC) curve of the hole-only devices in the dark (a), Time-resolved photoluminescence (TRPL) perovskite/HTM bilayer films (d).

The photovoltaic properties of the synthesized HTMs were studied in PSCs with a classic configuration: ITO/SnO_2/PCBA/$MAPbI_3$/**HTM**/MoO_x/Ag. The current-voltage characteristics of the champion cells are displayed in **Figure 4a**, while the current densities were confirmed by EQE spectra (Figure 4b). The device parameters are summarized in Table 2.

Table 2. Photovoltaic Parameters of PSCs in configuration ITO/SnO_2/PCBA/$MAPbI_3$/**HTM**/MoOx/Ag using different HTMs, in the form of maximum (average ± standard deviation).

HTM	V_{OC}, [mV]	J_{SC}, [mA/cm^2]	FF, [%]	PCE, [%]
TPA-t	1100 (1090±10)	23.0 (21.9±0.7)	69 67±2	17.4 (15.9±1.4)
TPA-t EH	1080 (1060±20)	22.3 (21.9±0.7)	67 (63±4)	16.1 (14.9±1.1)
PTAA	1000 (1005±9)	23.5 (22.0±1.0)	74 (72±2)	17.4 (16.0±1.4)

*The parameters were obtained from average 16 individual cells based on each HTM.

The results indicated that devices constructed with **TPA-t** and **TPA-t EH** materials possess increased open-circuit voltages compared to PTAA, with V_{OC} 1100, 1080, and 1000 mV respectively, outperforming reference significantly for 100 mV. This well agrees with HOMO levels, supporting the requirement for energy alignment. The short-circuit current in these devices was slightly lower than that of PTAA, approaching to J_{SC} 23.0, 22.3, and 23.5 mA/cm^2. The fill factor of devices with small molecular weight HTLs (67-69%) was lower than that for PTAA (74%) suggesting lower internal resistance in reference devices. However, despite these shortcomings, **TPA-t** devices maintain efficiencies comparable to a reference system and achieve 17.3%, whereas PTAA reaches 17.4%. Devices based on **TPA-t EH** were less effective, achieving only 16.1%. Relatively low short-circuit currents and fill factors may be due to recombination processes that occur either at the interface or within the bulk film.

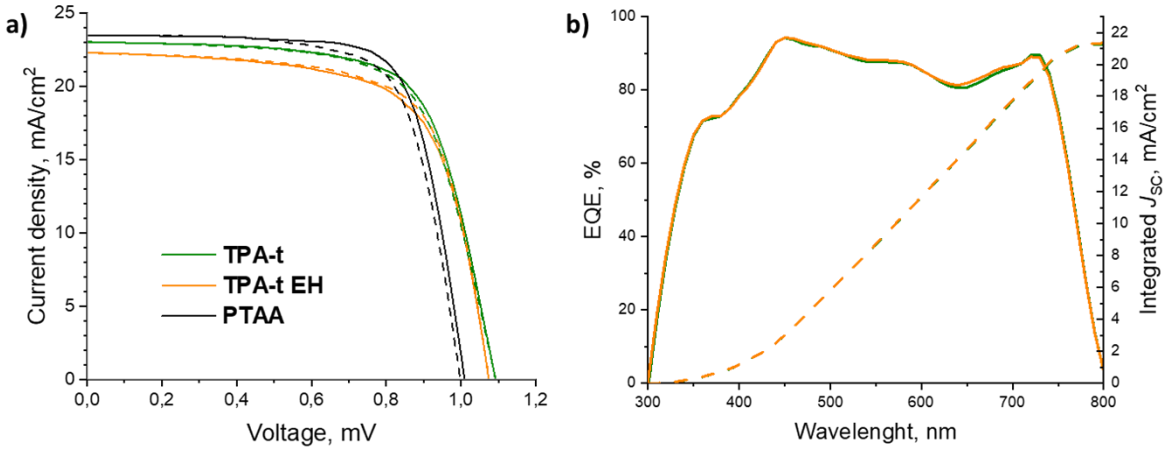

Figure 4. *J*–V curves forward (solid line) and reverse (dashed line) scans (a), External Quantum Efficiency (EQE) spectra (b).

The following analysis focuses on charge recombination mechanisms and their impact on solar cell performance. To understand the recombination mechanisms at open circuit, the incident light intensity effect on V_{OC} was measured (**Figure S2)**. The V_{OC} dependence on light intensity can be explained by the equation $V_{OC} \sim n_{id} \frac{k_B T}{q} \ln (P_{light})$. In this equation, n_{id} - represents the ideality factor, k_B - is the Boltzmann constant, T - is the absolute temperature, and q - is the elementary charge. Generally, an ideality factor of 1 indicates a primary band-to-band radiative recombination, while a value of 2 suggests a larger effect of trap-assisted Shockley–Read–Hall (SRH) recombination.[37] The ideality factors for the device based on **TPA-t** and **TPA-t EH** are 1.96 and 1.86, respectively. Therefore, these devices are predominantly influenced by trap-assisted recombination mechanisms. By comparing the ideality factors, we can deduce that **TPA-t EH** has fewer traps, which is evidenced by its higher mobility.

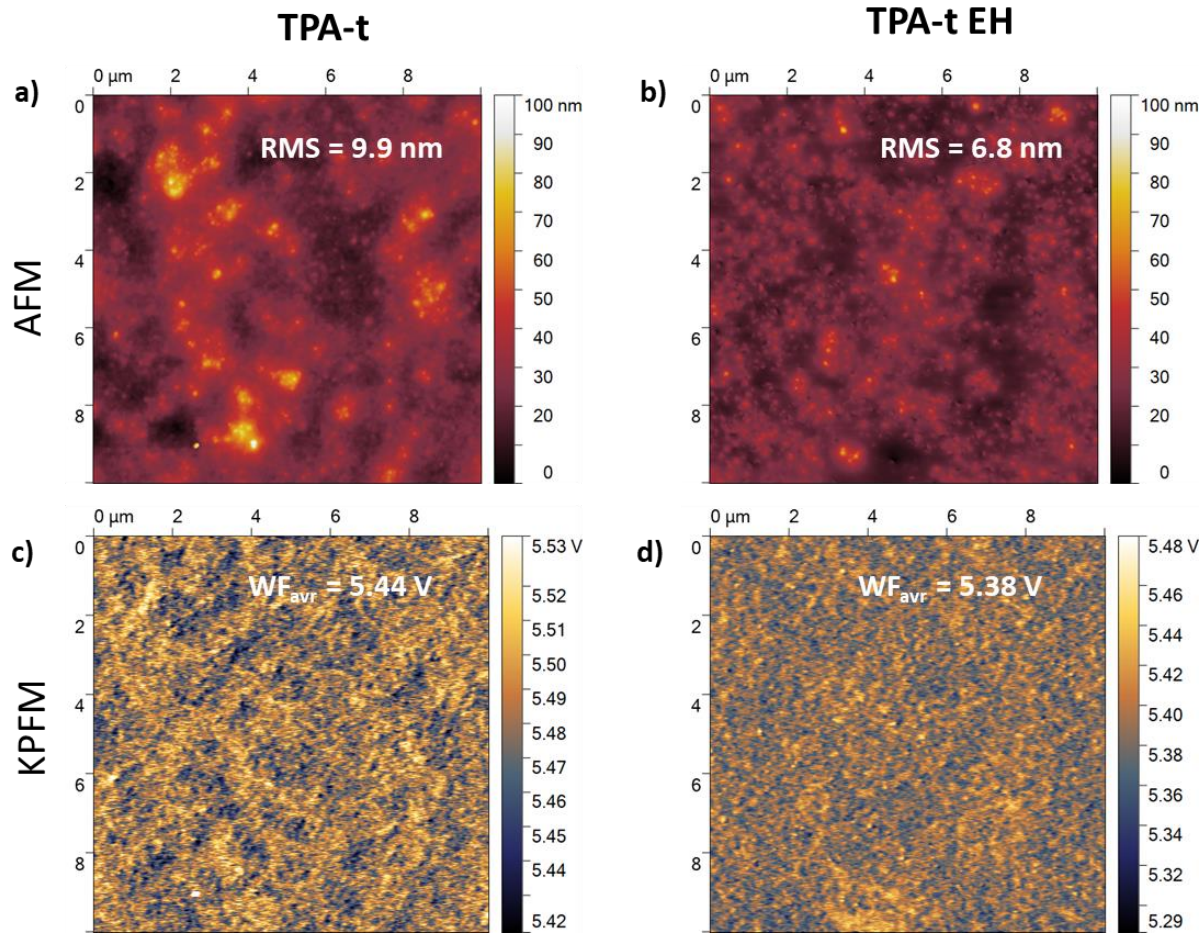

Figure 5. AFM images scaled in a range of (0–100 nm) and KPFM images showing the absolute values of WF for substrates glass/perovskite/HTM.

The next step involved investigating the morphology of HTMs in thin films formed atop perovskite. This was done using atomic force microscopy and Kelvin probe force microscopy

(KPFM) to measure the surface morphology and surface work function of ITO/$MAPbI_3$/**HTM** samples **Figure 5**. The RMS roughness of HTM films was found to be 9.9 and 6.8 nm for **TPA-t** and **TPA- t EH**, respectively. At first time, these films appear homogeneous. However, a closer look at the phase image reveals a pinhole in the **TPA-t EH** film (Figure S3). This could lead to low shunt resistance and subsequently a decrease in the fill factor. The work function of the surface was calculated from the potential of the reference highly oriented pyrolytic graphite (HOPG, WF = -4.6 eV). We also investigated samples with bare perovskite using this set of techniques and found the work function (WF) to be -4.9 eV. According to the KPFM data, the work function of the investigated materials equaled -5.44 and -5.38 for **TPA-t** and **TPA-t EH** respectively. In both cases, the work function was distributed evenly.

Conclusion

Two novel materials based on TPA core were synthesized and studied as HTLs in perovskite solar cells. The unique structural characteristics achieved by incorporating the triisopropylsilyl side chain into TPA have led to desirable properties. The two newly synthesized conjugated small molecules exhibit a low HOMO energy level of -5.38 and -5.31 eV for **TPA-t** and **TPA-t EH** respectively. Their HOMO levels align well with the energy levels of $MAPbI_3$, ensuring a reduction in energy losses during charge carrier transfer across the interface. As a result, we observed an increase in V_{OC} in devices up to 1.1 V, which is 100 mV higher than devices using PTAA as the hole transport material. Furthermore, these materials demonstrate excellent hole mobility and high charge extraction efficiency at the perovskite/HTL interface, achieving short-circuit currents of J_{SC} = 23.3 mA/cm^2. However, the lower fill factor compared to PTAA-based PSCs can likely be attributed to trap-assisted recombination and suboptimal morphology including pinhole. Despite these challenges, PSCs using TPA-t as HTL achieve high efficiency of undoped 17.4%, which is comparable to the PCE device using classic PTAA HTL. Given the benefits of conjugated small molecules over polymers, these synthesized CSM's show potential as a hole transport material for perovskite solar cells.

In conclusion, our research shows that strategically designing and modifying TPA-based materials with a triisopropylsilyl side chain is an effective method for creating innovative hole transporting materials.

Supporting Information

Supporting Information is available from the Wiley Online Library or from the author.

Acknowledgements

The research of small molecule applications in perovskite solar cells was supported of the Russian Science Foundation project № 23-73-01279. (https://rscf.ru/project/23-73-01279) The synthesis of small molecules is supported by the Ministry of Science and Higher Education of the Russian Federation 122111700041-8 (FFSG-2022-0004).

References

[1] N. Li, X. Niu, Q. Chen, H. Zhou, *Chem Soc Rev* **2020**, *49*, 8235.

[2] M. A. Green, E. D. Dunlop, | Masahiro Yoshita, N. Kopidakis, K. Bothe, G. Siefer, | Xiaojing Hao, **2023**, DOI 10.1002/pip.3750.

[3] NREL, *Best Research-Cell Efficiency Chart* **2019**.

[4] Z. Liang, Y. Zhang, H. Xu, W. Chen, B. Liu, J. Zhang, H. Zhang, Z. Wang, D.-H. Kang, J. Zeng, X. Gao, Q. Wang, H. Hu, H. Zhou, X. Cai, X. Tian, P. Reiss, B. Xu, T. Kirchartz, Z. Xiao, S. Dai, N.-G. Park, J. Ye, X. Pan, *Nature* **2023**, *624*, DOI 10.1038/s41586-023-06784-0.

[5] H. Zhu, S. Teale, M. N. Lintangpradipto, S. Mahesh, B. Chen, M. D. McGehee, E. H. Sargent, O. M. Bakr, *Nat Rev Mater* **2023**, *8*, DOI 10.1038/s41578-023-00582-w.

[6] A. S. R. Bati, Y. L. Zhong, P. L. Burn, M. K. Nazeeruddin, P. E. Shaw, M. Batmunkh, *Commun Mater* **2023**, *4*, DOI 10.1038/s43246-022-00325-4.

[7] A. K. Jena, A. Kulkarni, T. Miyasaka, *Chem Rev* **2019**, *119*, DOI 10.1021/acs.chemrev.8b00539.

[8] T. A. Chowdhury, M. A. Bin Zafar, M. Sajjad-Ul Islam, M. Shahinuzzaman, M. A. Islam, M. U. Khandaker, *RSC Adv* **2023**, *13*, DOI 10.1039/d2ra05903g.

[9] S. Khatoon, S. Kumar Yadav, V. Chakravorty, J. Singh, R. Bahadur Singh, M. S. Hasnain, S. M. M. Hasnain, *Mater Sci Energy Technol* **2023**, *6*, DOI 10.1016/j.mset.2023.04.007.

[10] Y. Wang, L. Duan, M. Zhang, Z. Hameiri, X. Liu, Y. Bai, X. Hao, *Solar RRL* **2022**, *6*, DOI 10.1002/solr.202200234.

[11] F. M. Rombach, S. A. Haque, T. J. Macdonald, *Energy Environ Sci* **2021**, *14*, DOI 10.1039/d1ee02095a.

[12] R. J. E. Westbrook, T. J. Macdonald, W. Xu, L. Lanzetta, J. M. Marin-Beloqui, T. M. Clarke, S. A. Haque, *J Am Chem Soc* **2021**, *143*, DOI 10.1021/jacs.1c05122.

[13] M. Stolterfoht, P. Caprioglio, C. M. Wolff, J. A. Márquez, J. Nordmann, S. Zhang, D. Rothhardt, U. Hörmann, Y. Amir, A. Redinger, L. Kegelmann, F. Zu, S. Albrecht, N. Koch, T. Kirchartz, M. Saliba, T. Unold, D. Neher, *Energy Environ Sci* **2019**, *12*, DOI 10.1039/c9ee02020a.

[14] I. Gelmetti, N. F. Montcada, A. Pérez-Rodríguez, E. Barrena, C. Ocal, I. García-Benito, A. Molina-Ontoria, N. Martín, A. Vidal-Ferran, E. Palomares, *Energy Environ Sci* **2019**, *12*, DOI 10.1039/c9ee00528e.

[15] I. V. Martynov, A. Akkuratov, P. A. Troshin, I. Visoly-Fisher, E. A. Katz, *Sustain Energy Fuels* **2022**, *6*, 2727.

[16] P. Yan, D. Yang, H. Wang, S. Yang, Z. Ge, *Energy Environ Sci* **2022**, *15*, DOI 10.1039/d2ee01256a.

[17] L. Zhang, X. Zhou, C. Liu, X. Wang, B. Xu, *Small Methods* **2020**, *4*, DOI 10.1002/smtd.202000254.

[18] I. E. Kuznetsov, A. A. Piryazev, A. F. Akhkiamova, M. E. Sideltsev, D. V. Anokhin, A. V. Lolaeva, M. V. Gapanovich, D. S. Zamoretskov, D. K. Sagdullina, M. V. Klyuev, D. A. Ivanov, A. V. Akkuratov, *ChemPhysChem* **2023**, *24*, DOI 10.1002/cphc.202300310.

[19] M. E. Sideltsev, A. A. Piryazev, A. F. Akhkiamova, M. V. Gapanovich, D. V. Anokhin, D. K. Sagdullina, A. S. Novikov, D. A. Ivanov, A. V. Akkuratov, *Physica Status Solidi - Rapid Research Letters* **2023**, DOI 10.1002/pssr.202300223.

[20] Y. N. Luponosov, A. N. Solodukhin, A. L. Mannanov, P. S. Savchenko, Y. Minenkov, D. Y. Paraschuk, S. A. Ponomarenko, *Dyes and Pigments* **2020**, *177*, 108260.

[21] Y. N. Luponosov, A. N. Solodukhin, A. L. Mannanov, P. S. Savchenko, B. A. L. Raul, S. M. Peregudova, N. M. Surin, A. V. Bakirov, M. A. Shcherbina, S. N. Chvalun, M. S. Pshenichnikov, D. Y. Paraschuk, S. A. Ponomarenko, *Mater Today Energy* **2021**, *22*, 100863.

[22] D. O. Balakirev, Y. N. Luponosov, A. L. Mannanov, P. S. Savchenko, Y. Minenkov, D. Y. Paraschuk, S. A. Ponomarenko, *Dyes and Pigments* **2020**, *181*, 108523.

[23] I. E. Kuznetsov, D. V. Anokhin, A. A. Piryazev, M. E. Sideltsev, A. F. Akhkiamova, A. V. Novikov, V. G. Kurbatov, D. A. Ivanov, A. V. Akkuratov, *Physical Chemistry Chemical Physics* **2022**, *24*, DOI 10.1039/d2cp01758j.

[24] Z. Chen, P. Cai, J. Chen, X. Liu, L. Zhang, L. Lan, J. Peng, Y. Ma, Y. Cao, *Advanced Materials* **2014**, *26*, DOI 10.1002/adma.201305092.

[25] A. V. Akkuratov, I. E. Kuznetsov, P. M. Kuznetsov, N. V. Tukachev, I. V. Martynov, S. L. Nikitenko, A. V. Novikov, A. V. Chernyak, A. Zhugayevych, P. A. Troshin, *Synth Met* **2020**, *259*, 116231.

[26] P. Zhou, D. Dang, M. Xiao, Q. Wang, J. Zhong, H. Tan, Y. Pei, R. Yang, W. Zhu, *J Mater Chem A Mater* **2015**, *3*, DOI 10.1039/c5ta00166h.

[27] M. Li, A. H. Balawi, P. J. Leenaers, L. Ning, G. H. L. Heintges, T. Marszalek, W. Pisula, M. M. Wienk, S. C. J. Meskers, Y. Yi, F. Laquai, R. A. J. Janssen, *Nat Commun* **2019**, *10*, DOI 10.1038/s41467-019-10519-z.

[28] A. Akkuratov, I. Martinov, I. Avilova, P. Troshin, *Physica Status Solidi - Rapid Research Letters* **2019**, *13*, DOI 10.1002/pssr.201900154.

[29] C. M. Cardona, W. Li, A. E. Kaifer, D. Stockdale, G. C. Bazan, *Advanced Materials* **2011**, *23*, 2367.

[30] K. J. Thorley, M. Benford, Y. Song, S. R. Parkin, C. Risko, J. E. Anthony, *Mater Adv* **2021**, *2*, DOI 10.1039/d1ma00447f.

[31] I. E. Kuznetsov, A. A. Piryazev, A. F. Akhkiamova, M. E. Sideltsev, D. V. Anokhin, A. V. Lolaeva, M. V. Gapanovich, D. S. Zamoretskov, D. K. Sagdullina, M. V. Klyuev, D. A. Ivanov, A. V. Akkuratov, *ChemPhysChem* **2023**, *24*, DOI 10.1002/cphc.202300310.

[32] P. N. Murgatroyd, *J Phys D Appl Phys* **1970**, *3*, DOI 10.1088/0022-3727/3/2/308.

[33] V. M. Le Corre, E. A. Duijnstee, O. El Tambouli, J. M. Ball, H. J. Snaith, J. Lim, L. J. A. Koster, *ACS Energy Lett* **2021**, *6*, DOI 10.1021/acsenergylett.0c02599.

[34] Y. Ko, Y. Kim, C. Lee, Y. Kim, Y. Jun, *ACS Appl Mater Interfaces* **2018**, *10*, DOI 10.1021/acsami.7b18745.

[35] J. P. Correa-Baena, W. Tress, K. Domanski, E. H. Anaraki, S. H. Turren-Cruz, B. Roose, P. P. Boix, M. Grätzel, M. Saliba, A. Abate, A. Hagfeldt, *Energy Environ Sci* **2017**, *10*, DOI 10.1039/c7ee00421d.

[36] Q. Cao, Y. Li, H. Zhang, J. Yang, J. Han, T. Xu, S. Wang, Z. Wang, B. Gao, J. Zhao, X. Li, X. Ma, S. M. Zakeeruddin, W. E. I. Sha, X. Li, M. Grätzel, *Sci Adv* **2021**, *7*, DOI 10.1126/sciadv.abg0633.

[37] W. Tress, M. Yavari, K. Domanski, P. Yadav, B. Niesen, J. P. Correa Baena, A. Hagfeldt, M. Graetzel, *Energy Environ Sci* **2018**, *11*, DOI 10.1039/c7ee02415k.

Our research shows that strategically designing and modifying TPA-based materials with a triisopropylsilyl side chain is an effective method for creating innovative hole transporting materials. These new molecules have HOMO levels aligning with $MAPbI_3$ energy levels, resulting in a V_{OC} increase in devices up to 1.1 V, and an efficiency of 17.4%, comparable to the classic PTAA HTL device.

Conjugated Small Molecules with Alkylsilyl-Modified Triphenylamine: A Promising Hole Transport Materials in Perovskite Photovoltaics.

ToC figure

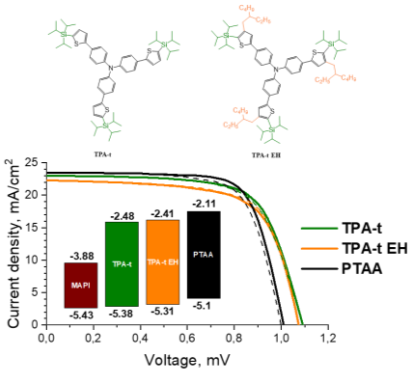

Supporting Information

Conjugated Small Molecules: A Promising Hole Transport Materials in Perovskite Photovoltaics

Materials and methods

Tris(4-bromophenyl)amine (compound 1)

Triphenylamine (1 g, 4 mmol) was dissolved in 20 mL of N,N-dimethylformamide and N-bromosuccinimide (0.726 g, 12 mmol, 3 eq.) was added in small portions. The mixture was stirred at room temperature for 6 hours, then poured into water. The precipitated white crystals were filtered and dried in air. Yield =98%. ^{1}H NMR (500 MHz, $CDCl_3$, δ, ppm): 7.37 (d, 6H); 7.31 (d, 6H) ppm.

Tris(4-(thiophen-2-yl)phenyl)amine (compound 2)

Solution of compound **1** (1.93 g, 4 mmol) in N,N-dimethylformamide (20 mL) was placed into 50 mL three-neck round-bottom flask equipped with reversed condenser. Then tributyl(thiophen-2-yl)stannane (4.48 g, 12 mmol, 3 eq.), and $Pd(PPh_3)_4$ (9 mg, 0.008 mmol) were added. The reaction mixture was stirred at 150°C for 12h under inert atmosphere. The mixture was cooled down to room temperature and the solvent was removed at the rotary evaporator. Purification was carried out using column chromatography using hexane as eluent. The yield of pure compound was 80%. ^{1}H NMR (500 MHz, $CDCl_3$, δ, ppm): 7.54 (d, 3H); 7.29 (d, 3H); 7.16 (d, 6H); 7.10 (t, 3H) ppm.

Tris(4-(5-(triisopropylsilyl)thiophen-2-yl)phenyl)amine (TPA-t)

Tris(4-(thiophen-2-yl)phenyl)amine (1.48 g, 3 mmol) was dissolved in 100 mL anhydrous THF in two-necked round-bottom flask under inert atmosphere. The mixture was cooled down to -78°C in acetone bath and 1.6 mL (4 mmol, 2.5 M in hexane) of n-BuLi was added dropwise through septum. After stirring at 0°C for 1h, 0.62 g (0.772 g, 4 mmol) chlorotriisopropylsilane was added slowly and the mixture stirred two hours at room temperature. The reaction was quenched with 25 mL water and extracted with ethylacetate in the separating funnel. The organic solution was dried over $MgSO_4$, filtrated, and solvent was removed at the rotary evaporator. The crude product was purified by column chromatography, using hexane, which

resulted in a pale yellow solid with a yield of 83%. ^{1}H NMR (500 MHz, $CDCl_3$, δ, ppm): 7.58 (d, 6H); 7.38 (d, 3H); 7.27 (d, 3H); 7.16 (d, 6H); 1.45 - 1.38 (m, 9H); 1.18 (d, 54H) ppm. ^{13}C NMR ($CDCl_3$, 126 MHz, δ): 149.11; 146.45; 136.74; 133.35; 129.31; 126.86; 124.37; 123.52; 18.65; 11.84 ppm.

3-(2-ethylhexyl)thiophene (compound 3)

3-bromothiophene (1) (56.2 g, 345 mmol), dichloro[1,3-bis(diphenylphosphino)propane] nickel (II) (Ni(dppp)Cl_2) (1.9 g, 0.01 eq.) and 100 mL of freshly distilled THF were placed into a 500 mL flask under argon flux. To the reaction mixture 2M (2-ethylhexyl)magnesium bromide solution in THF (172.5 mL 345 mmol) was added dropwise at 0 °C. The brown solution was stirred for 2h at room temperature. Then 20 mL of 2M hydrochloric acid was added and the resulting mixture was extracted three times with 50 mL of chloroform. The combined organic layer was washed with $NaHCO_3$ and brine, and the organic layer was dried over Na_2SO_4. After filtration, the solvent was removed by rotary evaporation and pale yellow oil was distilled under reduced pressure (1 mm Hg) giving 41 g of the pure title compound as a colorless oil. The yield was of 62 %. ^{1}H NMR (500 MHz, $CDCl_3$, δ, ppm): 7.22 (m, 1H); 6.92 - 6.87 (m, 2H); 2.57 (d, 2H); 1.57 - 1.52 (m, 1H); 1.31 - 1.18 (m, 8H); 0.88 (t, 6H) ppm.

2-bromo-3-(2-ethylhexyl)thiophene (compound 4)

N-bromosuccinimide (NBS) (121 mmol, 21.5 g) was added portionwise to a solution of 3-(2-ethylhexyl)thiophene (127 mmol, 25 g) in 100 mL mixture of chloroform and acetic acid (1:1 (v/v)), at 5 °C. The mixture was stirred at room temperature for 60 min. Then, 200 mL of H_2O was added, the chloroform layer was separated and washed with saturated solution of $NaHCO_3$ and distilled water. Organic solution was dried over Na_2SO_4, filtered and the solvent was removed by rotary evaporation to afford 33 g of product as a colorless oil. The yield of compound **4** was 94%.

^{1}H NMR (500 MHz, $CDCl_3$, δ, ppm): 7.21 (d, 1H); 6.80 (d, 1H); 2.54 (d, 2H); 1.67 - 1.62 (m, 1H); 1.35 - 1.22 (m, 8H); 0.94 (t, 6H) ppm.

(3-(2-ethylhexyl)thiophen-2-yl)triisopropylsilane (compound 5)

Solution of **4** (5 g, 18 mmol) in THF (70 mL) was placed into a 250 mL three-neck round-bottom flask, which was previously evacuated/backfilled with argon three times. The flask was then cooled to -78 °C in an acetone bath, and 2.5 M BuLi (18 mmol, 7.26 mL) was added dropwise. The reaction mixture was stirred at -60°C for 2 h. Then the solution of chlorotriisopropylsilane (3.82 g, 19.8 mmol) was added in one portion. The mixture was stirred at room temperature for 2 h. Then the solvent was removed using a rotary evaporator, producing a viscous oil, which was then distilled under reduced pressure (1 mm Hg) to give 4.82 g of the

pure title compound as a colorless liquid with a yield of 76%. ^{1}H NMR (500 MHz, $CDCl_3$, δ, ppm): 7.50 (d, 1H); 7.08 (d, 1H); 2.61 (d, 2H); 1.75 - 1.72 (m, 1H); 1.45 - 1.38 (m, 3H); 1.35 - 1.22 (m, 8H); 1.12 (d, 18H); 0.87 (t, 6H) ppm.

(3-(2-ethylhexyl)-5-(trimethylstannyl)thiophen-2-yl)triisopropylsilane (Compound 6)

(3-(2-ethylhexyl)thiophen-2-yl)triisopropylsilane (3.52 g, 10 mmol) in THF (50 mL) was placed into a 100 mL two-neck round-bottom flask, which was previously evacuated/backfilled with argon three times. The flask was then cooled to -78 °C in an acetone bath, and 2.5 M BuLi (10 mmol, 4 mL) was added dropwise. The reaction mixture was stirred at 0°C for 2 h. Then the solution of chlorotrimethylstannane (2.19 g, 11 mmol) in THF(5 mL) was added in one portion. The mixture was stirred at room temperature for 2 h. The solvent was removed at the rotary evaporator producing a viscous oily residue. The crude product was used in the next step without further purification. The yield of **6** was 90%. ^{1}H NMR (500 MHz, $CDCl_3$, δ) 7.18 (s, 1H); 2.70 (d, 2H); 1.65(m, 1H); 1.25-1.45 m (8H); 1.12 (m, 21H); 0.91 (t, 6H); 0.37 (s, 9H) ppm

Tris(4-(4-(2-ethylhexyl)-5-(triisopropylsilyl)thiophen-2-yl)phenyl)amine (TPA-t EH)

Solution of compound **1** (0.48 g, 1 mmol, 1 eq.) in N,N-dimethylformamide (20 mL) was placed into 50 mL three-neck round-bottom flask equipped with reversed condenser and thermometer. Then compound **6** (1.55 g, 3 mmol, 3 eq.), and $Pd(PPh_3)_4$ (9 mg, 0.008 mmol) were added. The reaction mixture was stirred at 150°C for 12h under inert atmosphere. The mixture was cooled down to room temperature and the solvent was removed at the rotary evaporator. The crude product was dissolved in 10 mL of toluene and filtered through a syringe filter (PTFE, 0.45 μm). The solution was processed further using a preparative Phenogel GPC column (21.2 mm × 300 mm) and acetonitrile as eluent. The yield of TPA-t EH was 69%. ^{1}H NMR (500 MHz, $CDCl_3$, δ, ppm): 7.49 (d, 6H); 7.22 (s, 3H); 7.08 (d, 6H); 2.58 (d, 6H); 1.75 - 1.72 (m, 3H); 1.45 - 1.38 (m, 9H); 1.35 - 1.22 (m, 24H); 1.12 (d, 54H); 0.87 (t, 18H) ppm. ^{13}C NMR ($CDCl_3$, 126 MHz, δ): 150.94; 147.47; 146.35; 129.39; 128.35; 126.58; 125.49; 124.29; 40.16; 36.72; 32.94; 29.12; 26.13; 23.08; 19.06; 14.15; 13.10; 11.18.

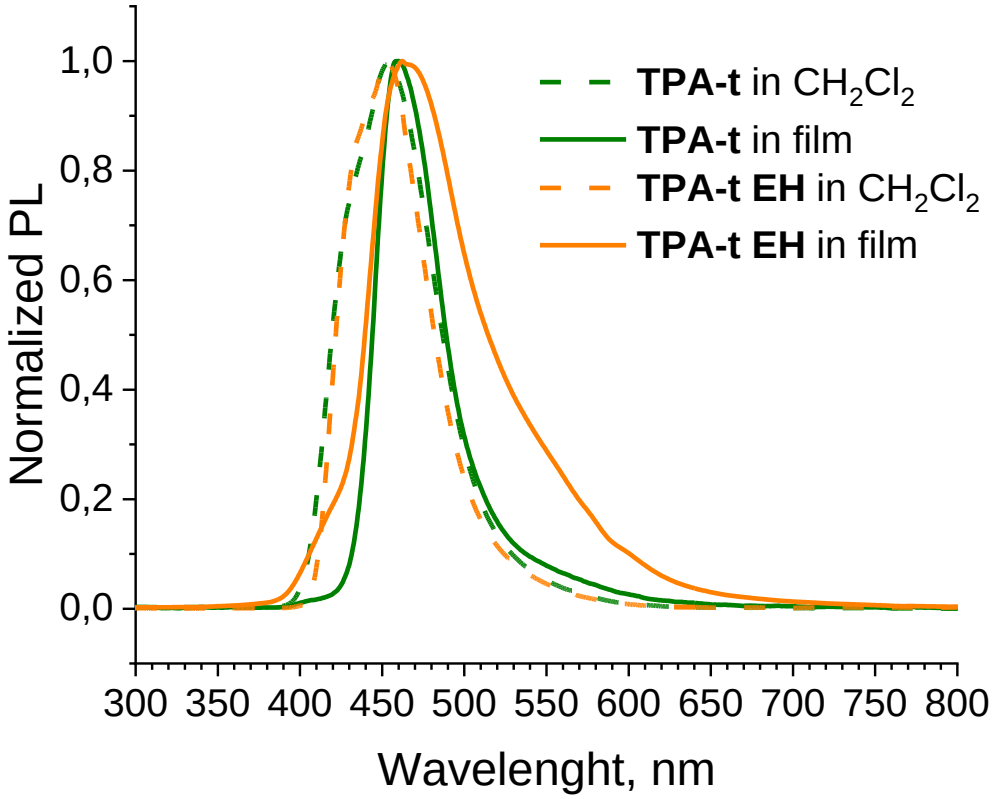

Figure. S1 Photoluminescence spectra in solution and thin films of **TPA-t** and **TPA-t EH.**

Table. S1 Parameters of bi-exponential model fitting of TRPL.

HTL	**A_1**	**τ_1**	**A_2**	**τ_2**	**$\tau_{average}$**
$MAPbI_3$	0.5	20	0.4	115	98.1
TPA-t	0.3	7	0.6	36	33.4
TPA-t EH	0.4	19	0.5	125	113.5

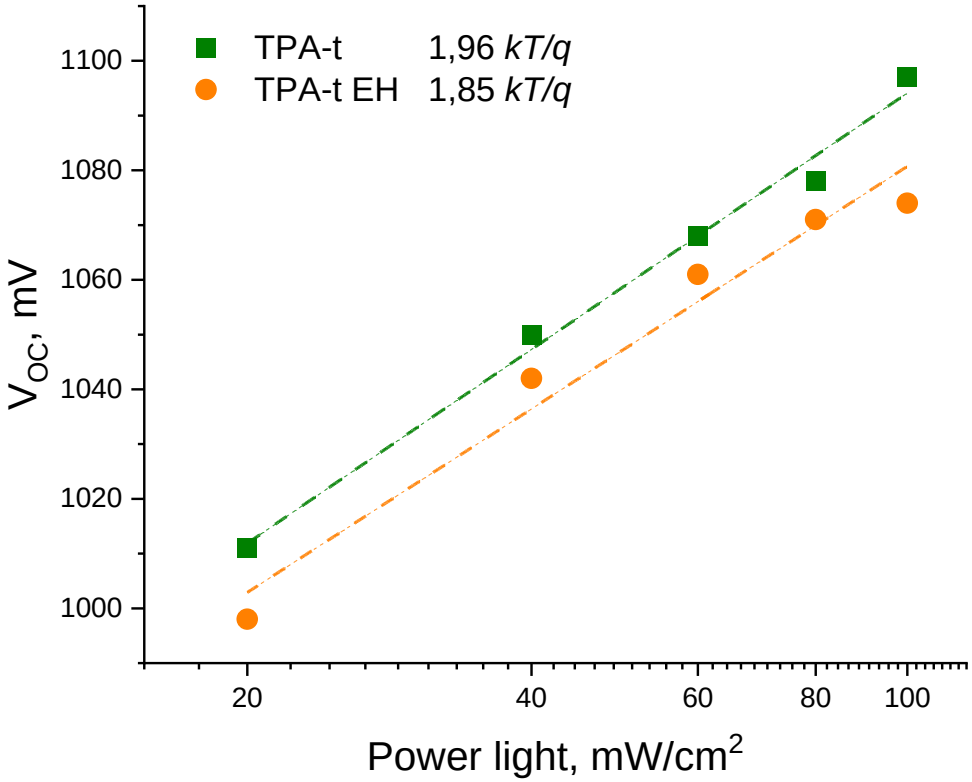

Figure S2. The open-circuit voltage is dependent on the light power for devices based on TPA- t and TPA-t EH. The corresponding light ideality factors are provided in the legends.

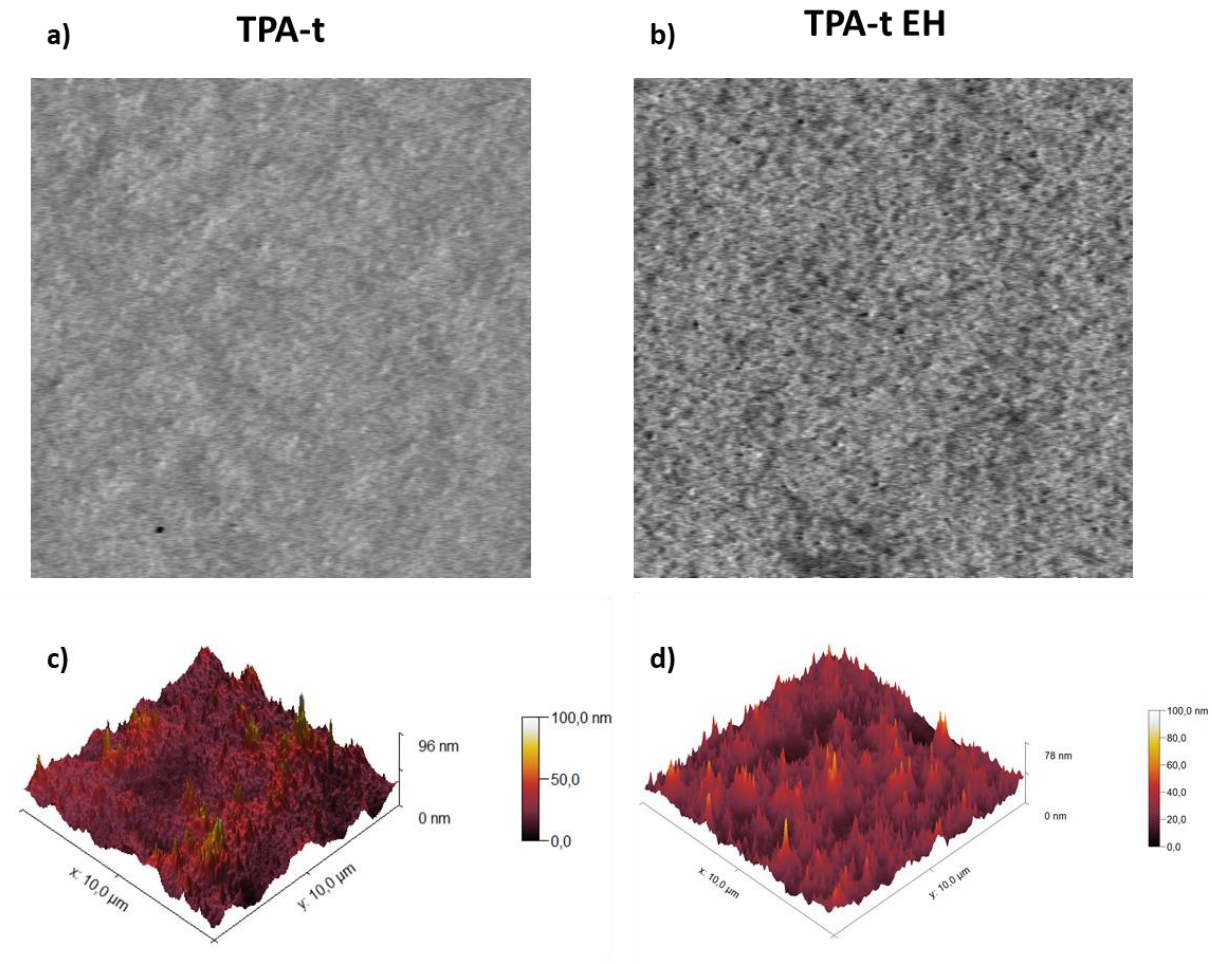

Figure S3. AFM image bilayer thin films TPA- t and TPA-t EH, glass/perovskite/HTM phase mode (a,b) and 3D topology (c,d).